

Macroscopic Order and Electro-Optic Response of Dipolar Chromophore–Polymer Materials

Yuriy V. Pereverzev, Oleg V. Prezhdo,* and Larry R. Dalton^[a]

This Minireview considers the key factors that govern the organization of macroscopic polarization in nonlinear optical systems obtained by electric poling of organic dipolar chromophores dissolved in polymer matrices. The macroscopic electric polarization depends on the thermodynamic state of the dipole system. The dependence of the paraelectric and antiferroelectric states of dipolar chromophores on the chromophore concentration and the strength of the poling field is discussed. Phase transitions between the para- and antiferroelectric states are investigated within the limits of the Ising and isotropic models for the chro-

mophore dipoles and are considered for varying chromophore concentration, poling field strength, and macroscopic shape of the sample used for poling. The macroscopic polarization and electro-optic coefficient of the material change drastically upon phase transition. The theories are compared with the experimental data on the electro-optic coefficient dependence on the chromophore concentration. The isotropic dipole model shows excellent agreement with experiment for the chromophore systems most commonly used in nonlinear optics.

1. Introduction

The design and investigation of organic nonlinear optical (NLO) materials are driven by applications in a great variety of optical devices including, for example, fiber-optic transmission lines and amplifiers, electrical-to-optical signal transducers for cable television, diode lasers, high-density memories, flat panel displays and biomedical voltage sensors.^[1–16] The improvement of existing organic NLO materials and the design of novel materials involve two major steps on both microscopic and macroscopic levels:

First, molecular or macromolecular structures are constructed based on organic, π -conjugated chromophores, enhanced with various donor and acceptor moieties.^[17] The chromophore fragments are then introduced into polymers either as guests, side groups, or main chain segments. Individual chromophores are chemically bonded into well-defined structures, such as cone supramolecules and dendrimers,^[15, 16, 18, 19] in which dipole moments and NLO effects add up with the number of connected chromophores. The microscopic NLO fragments can be additionally enhanced with cross-linkable groups that, at moderately high temperatures or by the application of light, interact and form stable, cross-linked polymeric networks.^[15, 20, 21]

Second, the microscopic NLO elements are organized on a macroscopic level to exhibit the desired NLO properties. In many cases, in order to be optically active on the macroscopic scale, materials must be polarized by a particular spatial ordering of the microscopic structural elements. For instance, the desired spatial order can be achieved in Langmuir–Blodgett films and self-assembled superlattices.^[22–26] More generally, and often most efficiently, the microscopic molecular NLO elements are designed to possess large dipole moments that are ordered by an external field.^[27–33]

The current Minireview follows our earlier work^[19, 34–37] and, using the existing theories of dipolar ordering, describes the key factors that determine the efficiency of poling in the formation of macroscopic polarization in NLO materials.

This Minireview is organized in the following way: Section 2 considers the poling process in more detail, focusing on general strategies. The poling efficiency for systems of noninteracting dipoles corresponding to the low chromophore concentration limit is investigated. The resulting macroscopic polarization and electro-optic (EO) coefficient are shown to depend strongly on the space of available dipole orientations. The anisotropic nature of the dipole–dipole interaction is illustrated by the dipole correlation function. The effect of the chromophore shape on the dipole–dipole interaction and the resulting spatial and orientation order is discussed.

Section 3 describes the Ising model for the dipole–dipole interaction. The thermodynamic states in the system of Ising dipoles are investigated, and equations for the phase transition lines are given. The EO coefficient is calculated as a function of the external and microscopic parameters. Section 4 carries out a similar analysis for the isotropic dipole–dipole interaction model. The effect of the macroscopic shape of the sample on poling efficiency is illustrated with both Ising and isotropic models. The theoretical results and predicted dependencies of the EO coefficient on the experimentally variable parameters are discussed and compared with the experimental data for four chromophore types in Section 5. The Minireview concludes with a summary of the key results.

2. Strategies for Improved Poling Efficiency

The first molecular hyperpolarizability β is responsible for the Pockels effect that allows the refraction index of a material to be controlled by applying a weak external electric field. The

[a] Dr. Y. V. Pereverzev, Prof. O. V. Prezhdo, Prof. L. R. Dalton
Department of Chemistry, University of Washington
Seattle, WA 98195-1700 (USA)
Fax: (+1) 206-685-8665
E-mail: prezhdo@u.washington.edu

Pockels effect is a second-order NLO phenomenon where the two fields are the optical and control fields. If chromophores are placed randomly in the bulk, the average over chromophore orientations results in cancellation of the even-order polarization effects, including the Pockels effect, even though the chromophores themselves have no center of symmetry. Only a noncentrosymmetric ordering of chromophores translates large hyperpolarizabilities of individual molecules into a macroscopic EO response of a molecular ensemble.

Dipole moments of the chromophores used in the EO materials based on the Pockels effect are of the order of 10–15 Debye and point in the direction of the longest molecular axis.^[17] The chromophore molecules are dissolved in a melted polymer matrix at temperatures T above the polymer glass transition temperature T_g , $T > T_g$. The macroscopic order in the molecular ensemble is achieved by applying an external electric field E . The alignment is preserved by lowering T below T_g or by chemical cross-linking of the chromophore–polymer mixture. Note that the values of the chromophore dipoles are assumed constant during the poling process, independent of the applied field.

The polymer medium containing dipolar chromophores creates thermal noise that acts to destroy the order produced by the poling field. In addition, polymers interact with chromophores by chemical, van der Waals and other interactions. Local anisotropy in the chromophore–polymer interaction restricts the space of states available to chromophore dipoles. For instance, chemical bonding between chromophores and polymers may favor certain directions of the chromophore axis. Short-range repulsive chromophore–polymer and chromophore–chromophore interactions may create liquid-crystalline local order leading to correlations in orientations, or in both orientations and positions of chromophore molecules.

If chromophores are unconstrained by chromophore–polymer interactions, the chromophore dipole moments can take all possible orientations in the three dimensional space, Figure 1. The Hamiltonian of the interaction between the chromophore dipole $\vec{\mu}$ and the poling field \vec{E} is $H_E = -\mu_z E / \epsilon$, where ϵ is the polymer dielectric constant. The dipole order parameter σ determines polarization per chromophore $p_z = \mu\sigma$ and is defined by the thermodynamic average given in Equation (1):

$$\sigma = \langle \mu_z \rangle / \mu = (e' \cosh e' - \sinh e') / e' \sinh e' \quad (1)$$

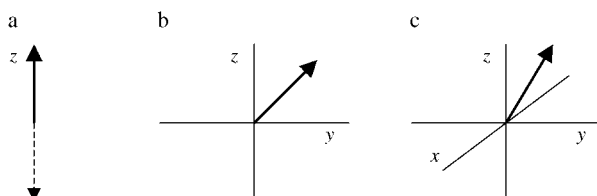


Figure 1. Allowed states of chromophore dipoles in a) Ising, b) planar, and c) isotropic dipole models. The poling field is applied along the z-axis. The dipole moment, bold arrow, has only two states in the Ising model, pointing either up or down. The dipole can freely rotate within a plane in the planar model and within the three-dimensional space in the isotropic model.

where μ is the magnitude of the molecular dipole moment, $e = \mu E / k_B T$ is the dipole–field interaction energy μE in units of thermal energy $k_B T$, $e' = e / \epsilon$ is the dipole–field interaction attenuated by the polymer dielectric constant ϵ , and k_B is the Boltzmann constant. It follows from Equation (1) that $\sigma = 0$ when $e = 0$ and that $\sigma \rightarrow 1$ as $e \rightarrow \infty$.

Chromophores can be chemically bonded to polymer chains and remain roughly perpendicular to the chain. Rotational flexibility of polymer chains, for example, by rotation around single carbon–carbon bonds allows chromophore dipoles to rotate in the plane perpendicular to the chain. Spin-coating of polymer films places such polymer chains perpendicular to the poling field. Then, the thermodynamic average, Equation (1) equals Equation (2):

$$\sigma = I_1(e') / I_0(e') \quad (2)$$

where $I_n(e')$ is the modified Bessel function of order n .

Finally, liquid-crystalline local chromophore order can be created by chromophore–chromophore and chromophore–polymer hard-core repulsive and van der Waals interactions, restricting the space of states available to dipoles to only two states, up and down. The two state space leads to an Ising model, Equation (3):

$$\sigma = \tanh e' \quad (3)$$

Figure 1 illustrates the states accessible by chromophore dipoles for unconstrained chromophores, chromophores chemically bonded to spin-coated polymer chains, and chromophores in liquid-crystalline phases. Figure 2 shows the depend-

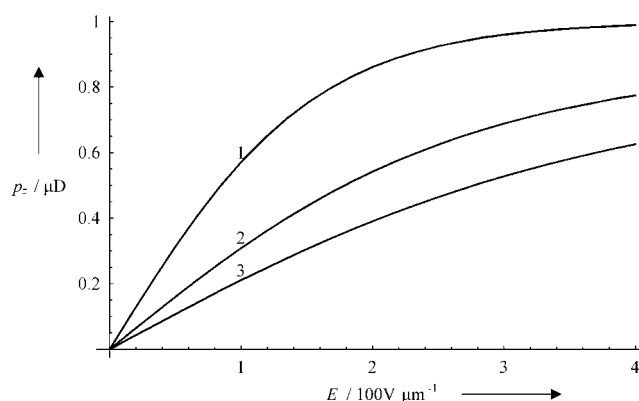


Figure 2. Macroscopic polarization p_z per chromophore in a system of non-interacting chromophore dipoles subject to a poling field and thermal disorder as a function of the field strength E . Curves 1, 2, and 3 correspond to the Ising, planar, and isotropic models. For a given field strength, the polarization is larger if the space of dipole states is smaller. The data are presented for $\mu = 10$ D, $T = 373$ K, $E = 100$ $V \mu\text{m}^{-1}$, $\epsilon = 1$.

ence of the polarization per chromophore $p_z = \mu\sigma$ on the strength of the poling field E in these three cases. Restriction of the state space to fewer dimensions increases the macroscopic polarization.

Next, consider the magnitude of the EO coefficient for the isotropic, planar, and Ising models. A general expression for the EO coefficient $r_{33} \equiv r$ is given by Equation (4):

$$r(x) = x \langle \cos^3 \vartheta \rangle \quad (4)$$

where the angle ϑ describes the deviation of the chromophore dipole from the direction of the poling field, and $x = N/N_0$ is the reduced chromophore concentration defined by the ratio of the number of molecules per unit volume to $N_0 = 10^{20} \text{ cm}^{-3}$. For a system of noninteracting dipoles, the thermodynamic average $\langle \cos^3 \vartheta \rangle$ is independent of x , and r is a linear function of concentration x with a proportionality coefficient that depends on the dipole-field interaction strength e and orientations available to the dipole. The EO coefficients of the systems of noninteracting dipoles in the Ising, planar, and isotropic models are given in Equations (5a), (5b), and (5c), respectively:

$$r1(x) = x \tanh e' \quad (5a)$$

$$r2(x) = x [3I_1(e') + I_3(e')] / 4I_0(e') \quad (5b)$$

$$r3(x) = x [e'(6 + e'^2) \coth e' - 3(2 + e'^2)] / e'^3 \quad (5c)$$

Figure 3 illustrates the dependence of the EO coefficients r , given by Equation (5), on the chromophore concentration x . Similarly to the macroscopic polarization of Figure 2, the EO coefficient is greatest in the Ising system and smallest in the isotropic system. It is important to note that for typical values of the chromophore dipole, $\mu \approx 10 \text{ D}$, electric field $E \approx 100\text{--}300 \text{ V } \mu\text{m}^{-1}$ and temperature $T \approx 373 \text{ K}$, the ratio $\mu E/k_B T \approx 1$, indicating that the dipole-field interaction is strong and cannot be treated as a linear perturbation.

The experimental data^[11,14] for various types of chromophores as a function of chromophore concentration exhibit a linear regime only at relatively low concentrations. With increasing concentration, the $r(x)$ values become smaller than those predicted by the noninteracting dipole model. Further

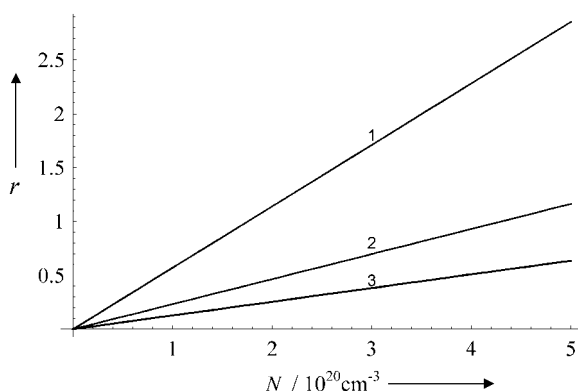


Figure 3. EO coefficient of a system of noninteracting dipoles as a function of chromophore number density, Equation (5). The EO coefficient is largest with Ising dipoles, curve 1, and decreases for planar, curve 2, and isotropic, curve 3, dipoles. The parameters are the same as in Figure 2.

concentration increase results in a maximum and subsequent decline in the EO coefficient. The deviation of $r(x)$ from linearity occurs due to dipole-dipole interaction between chromophores.

The dipole-dipole interaction is spatially anisotropic and contains a component that orders adjacent dipoles antiparallel. In order to illustrate this effect, consider the Hamiltonian of two interacting dipole moments $\vec{\mu}_1$ and $\vec{\mu}_2$ located a distance \vec{r} from each other. Within the two-state Ising model, the dipole-dipole interaction Hamiltonian takes the form $H_{dd} = \mu_{1z}\mu_{2z}(1 - 3\cos^2\Theta)/(4\pi\epsilon_0 r^3)$, where ϵ_0 is the permittivity of free space, Θ is the angle between the Ising axis and the radius vector \vec{r} , and μ_{1z} , μ_{2z} are the projections of the dipole moment on the Ising axis that can take the two values $\pm\mu$. It is straightforward to compute the thermally averaged correlation between the moments $\langle \mu_{1z}\mu_{2z} \rangle$ as a function of the angle Θ : $\langle \mu_{1z}\mu_{2z} \rangle = -\mu^2 \tanh[(1 - 3\cos^2\Theta)\alpha]$, where $\alpha = \mu^2/(4\pi\epsilon_0 r^3 k_B T)$. If Equation (6a) holds:

$$|\cos\Theta| > 1/\sqrt{3} \text{ or } \Theta < \Theta_0 = 54.74^\circ \text{ and } \Theta > \pi - \Theta_0 \quad (6a)$$

the adjacent dipoles point, on average, in the same direction and $\langle \mu_{1z}\mu_{2z} \rangle > 0$. On the contrary, if Equation (6b) is true:

$$|\cos\Theta| < 1/\sqrt{3} \text{ or } \pi - \Theta_0 > \Theta > \Theta_0 \quad (6b)$$

the dipoles point in the opposite directions and $\langle \mu_{1z}\mu_{2z} \rangle < 0$.

Figure 4a shows the dependence of the correlation function $k = \langle \mu_{1z}\mu_{2z} \rangle / \mu^2$ on the angle Θ for various values of the dipole-dipole interaction strength parameter α . The latter depends on the interchromophore distance r and, therefore, changes with chromophore concentration x . Chromophore dipoles that are located at angles [Equation (6a)] relative to a selected dipole will be parallel to it. Chromophore dipoles located at angles defined in Equation (6b) will be antiparallel to the selected dipole, Figure 4b. These results hold with numerical modifications for the three-dimensional isotropic and two-dimensional planar models of interacting dipoles.

The shape of the chromophore molecule plays an important role in defining the interaction between the chromophore dipoles. Molecular shapes regulate nearest-neighbor chromophore arrangements and determine states available to the chromophore dipole. Elongated molecules interacting via short-ranged excluded volume and Gay-Berne forces^[38] tend to produce liquid-crystalline local structures, where the long molecular axes are aligned, and the intermolecular distances are significantly shorter perpendicular to the molecular axes than along the molecular axes. This type of nearest-neighbor structure favors antiparallel dipole-dipole correlations that can produce centrosymmetric chromophore dimers.^[3,39] At the same time, spherical and, even better, oblate- and disk-shaped molecules favor parallel correlations of dipoles and are considered best candidates for ferroelectric states.^[40-42]

The significance of the spatial arrangement of dipole carriers in the resulting macroscopic state of interacting dipoles was first demonstrated by Luttinger and Tisza,^[43] who showed that the most stable state of isotropic dipoles arranged on a cubic

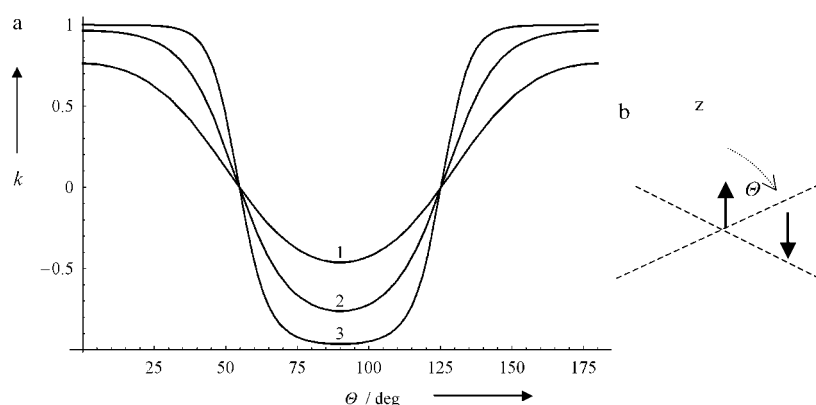


Figure 4. a) Dimensionless correlation function $k = \langle \mu_{1z} \mu_{2z} \rangle / \mu^2$ between two dipoles as a function of the angle Θ between the Ising axis and the radius vector connecting the two dipoles. The data are given for three values of the parameter $\alpha = \mu^2 / (4\pi\epsilon_0 r^3 k_B T)$ reflecting the dipole–dipole interaction strength, $\alpha = 1, 2, 3$ as corresponding to curves 1, 2, and 3 in the figure. Dipole moments placed above each other favor ferroelectric alignment, whereas dipoles placed laterally prefer antiferroelectric alignment, (b). The transition between the two alignments occurs at $\Theta = 54.74$ degrees in the Ising model.

lattice is antiferroelectric (AFE), whereas the ground state of dipoles on volume-centered and face-centered lattices is ferroelectric. The analysis summarized in Equations (6a) and (6b) agrees with these results. The present study focuses on the experimental work carried out with elongated chromophores^[10,11,14] that facilitate chemical generation of large molecular dipoles. It is expected that increases in chromophore concentration will emphasize the AFE correlations between chromophore dipoles, resulting in AFE states at high chromophore concentrations.

Last but not the least, it is important to note that the macroscopic polarization achieved by poling strongly depends on the macroscopic shape of poled samples. The electric field generated by chromophore dipoles is long-ranged. Chromophore dipoles aligned by the poling field create a depolarization field that opposes the poling field. The depolarization field is generated at the sample boundary and, therefore, depends on the sample shape.^[44] The magnitude of the depolarization field is proportional to the macroscopic polarization created in the sample and, therefore, is proportional to the concentration of chromophore dipoles.

The current work investigates the effect of the dipole–dipole interaction on the macroscopic polarization for the Ising and isotropic models using a self-consistent mean-field approach. As discussed above, the choice of these models was motivated by the spatial orientations available to individual chromophore dipoles.

3. The Ising Model

The Ising model describes the ordering of chromophore dipoles in the cases where molecular dipoles are allowed only two orientations, for instance, due to a pre-existing liquid-crystalline spatial chromophore order or when chromophores align parallel to polymer chains. Chromophore alignment along a preferred direction is best described by nematic anisotropy D with the Hamiltonian $H_a = -D\mu_z^2$. Comparison of the thermodynamic average $\langle \mu_z^2 \rangle$ computed using this Hamiltonian with the

averages $\langle \mu_x^2 \rangle = \langle \mu_y^2 \rangle$ indicates whether the Ising model is suitable. The average of $\langle \mu_z^2 \rangle$ must be much greater than the average of $\langle \mu_x^2 \rangle, \langle \mu_y^2 \rangle$. This condition is satisfied when $D\mu^2/k_B T > 4$.

The short-ranged excluded volume and Gay–Berne forces between chromophores or chromophores and polymers are much stronger than the long-ranged dipole–dipole forces and can produce nematic or smectic chromophore order.^[45] The nematic anisotropy D is proportional to the Gay–Berne interaction strength. The dipole–dipole interaction in the presence of an existing orientation and spatial

chromophore order is allowed with only two dipole orientations, parallel and antiparallel to the polymer chain or the nematic phase axis.

The Ising dipole–dipole interaction Hamiltonian in a uniform poling field is given by Equation (7):

$$H_d = \frac{\mu^2}{8\pi\epsilon_0\epsilon} \sum_{l \neq m} \left(1 - \frac{3r_{lmz}^2}{r_{lm}^2} \right) \frac{\mu_{lz} \mu_{mz}}{r_{lm}^3} - \frac{\mu E}{\epsilon} \sum_l \mu_{lz} \quad (7)$$

where \vec{r}_{lm} is the radius vector between dipoles l, m , and r_{lmz} is its projection on the Ising axis. Chromophore molecules are located at random in a nematic state. For simplicity, in order to avoid additional averaging over positions of chromophore molecules, it is assumed that the molecules are distributed on a simple cubic lattice with the lattice constant $a = N_0^{-1/3} \chi^{-1/3}$.

The electrostatic order in the above model is investigated in the self-consistent field approximation that reduces the many-body problem to a one-particle description.^[34–36] The number of one-particle Hamiltonians is determined by the number of dipolar sublattices required to describe a given thermodynamic state. In particular, a single sublattice describes the paraelectric (PE) state, whereas the AFE state requires two sublattices. The dipole moments of the chromophores in each sublattice interact with the effective field E_{eff} comprised of the following four contributions: the external field, the local field \vec{E}_l , the Lorentz field \vec{E}_L and the depolarization field \vec{E}_d . The separation of the fields acting on the selected dipole is general for mean-field models.^[46] Summation on a lattice is replaced by integration over the volume of the sample. A formal replacement of summation to integration diverges at the origin. In order to avoid the divergence, the summation is carried out explicitly over a small volume of the sample around the selected dipole. The explicit summation over the small volume gives the local field \vec{E}_l . The shape of the small volume is arbitrary, but spherical is most conveniently chosen, the so-called Lorentz sphere. The external field polarizes the bulk material and generates surface charges both at the macroscopic boundary of the

sample and on the Lorentz sphere producing \vec{E}_d and \vec{E}_L . \vec{E}_d depends on the macroscopic shape of the sample described by a rotation ellipsoid that can be prolate or oblate, as characterized by the depolarization factor n ranging from 0 for needle, 1/3 for sphere, to 1 for slab.

At low chromophore concentrations, high poling fields, or high temperatures, a uniform system of chromophore dipoles arranged on a cubic lattice exists in a PE state. All dipoles are thermodynamically equivalent. The Hamiltonian describing a selected dipole located at zero takes the simple form of Equation (8):

$$H = -\mu_{0z} \mu E_{\text{eff}} / \varepsilon = -\mu_{0z} \mu (E - (n-1/3) \mu \sigma N_0 x / \varepsilon_0) / \varepsilon \quad (8)$$

The value $\sigma = \langle \mu_{0z} \rangle$ is thermodynamically averaged with the Hamiltonian in Equation (8), and characterizes polarization of a single dipole. A straightforward computation gives Equation (9):

$$\sigma = \tanh[(e - \pi(n-1/3)\eta\sigma x) / \varepsilon] \quad (9)$$

where $\eta = \mu^2 N_0 / (\pi \varepsilon_0 k_B T)$.

The dependence of σ on the chromophore concentration x appears in Equation (9) due to the concentration dependence of the depolarization field. The dashed lines in Figure 5 show the dependence of $p_z = \mu\sigma$ on x obtained by the numerical solution of Equation (9) for samples of several shapes. The lines in Figure 5 clearly demonstrate the influence of the macroscopic sample shape on the magnitude of dipolar polarization.

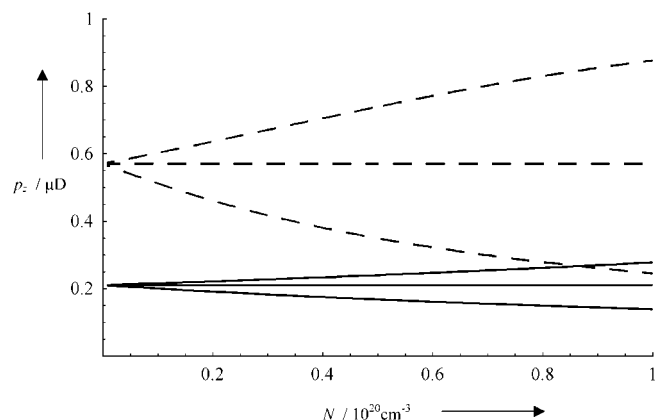


Figure 5. Polarization in the system of dipoles in the PE state computed per chromophore as a function of chromophore concentration. The dashed lines represent the Ising model, and the solid lines represent the isotropic model. The data for each model are considered for three shapes of the macroscopic sample: plate, sphere, and needle with $n = 1, 1/3$, and 0 from bottom to top, respectively, Equations (9) and (17). The polarization is independent from the chromophore concentration in spherically shaped samples ($n = 1/3$), grows with concentration in samples elongated along the poling field ($n < 1/3$), and decreases in oblate samples ($n > 1/3$). The polarization is significantly higher in the Ising model than in the isotropic model. This advantage of the Ising model is rapidly lost in plate shaped samples (lower dashed line). The parameters are the same as in Figure 2.

The normalized value of the EO coefficient for this model is given by Equation (10):

$$r = x\sigma \quad (10)$$

The concentration dependence $r(x)$ follows from Equations (10) and (9). An analytic dependence of r on x can be obtained in the high-temperature limit $\mu E_{\text{eff}} < \varepsilon k_B T$ that gives Equation (11):

$$r = x(1 + 2\pi\eta x / 3\varepsilon)^{-1} e / \varepsilon \quad (11)$$

It follows from Equation (11) that r is independent of x at high concentrations. Whether or not the concentration independent regime is achieved depends on the stability of the PE state with respect to the AFE phase transition.^[47]

The AFE state is the ground state of a cubic lattice of dipoles. The PE state becomes more favorable only due to the polarizing action of the poling field. Increasing dipole concentration emphasizes the AFE component of the dipole-dipole interaction relative to the dipole-poling field interaction, and the dipole system spontaneously transforms into the AFE state.

In contrast to the PE state, the ensemble averaged value of the dipole moment in any lattice site does not vanish in the AFE state even in the absence of the field, but the macroscopic polarization of the whole sample is zero, since the sub-lattices of the AFE state are polarized in opposite directions.

The Hamiltonian in Equation (7) produces an AFE state with dipoles forming ferroelectric chains that are ordered antiferroelectrically with respect to each other,^[48] as illustrated in Figure 6a. Similarly to antiferromagnetics,^[49,50] this order can be described by two effective fields, Equation (12):

$$E_{k\text{eff}} = E - (n-1/3)N_0\mu\sigma x / \varepsilon_0 - (-1)^k \mu N_0 x (\sigma_1 - \sigma_2) / (\pi\varepsilon_0) \quad (12)$$

where $k = 1, 2$ and σ_1, σ_2 , and σ are given by Equations (13a)–(13c):

$$\sigma_1 = \langle \mu_{1z} \rangle \quad (13a)$$

$$\sigma_2 = \langle \mu_{2z} \rangle \quad (13b)$$

$$\sigma = (\sigma_1 + \sigma_2) / 2 \quad (13c)$$

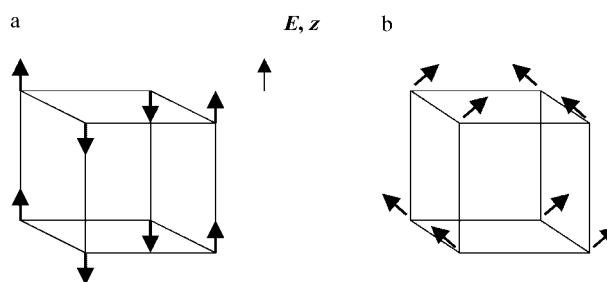


Figure 6. Structures of the AFE states in the systems of dipolar chromophores subject to a poling field in the z direction for a) the Ising model and b) the isotropic model.

Equations (13a)–(13c) describe both the AFE and PE states considered above. The PE state is obtained by setting $\sigma_1 = \sigma_2$. The system in Equations (13) is conveniently written in terms of the polarization variable σ and the AFE order parameter $l = (\sigma_1 - \sigma_2)/2$, Equations (14a) and (14b):

$$\sigma = \sqrt{1 + l^2 - 2l \coth(4lx\eta/\epsilon)} \quad (14a)$$

$$e = \pi(n-1/3)\eta\sigma x - 2\eta lx + 0.5\epsilon \ln[(1 + \sigma + l)/(1 - \sigma - l)] \quad (14b)$$

The variables σ and l change within the (0,1) range. The regions of the PE and AFE states are separated in the (x, e) plane by a line of second-order phase transitions. The equation for the phase transition line is obtained from Equation (14) in the limit $l \rightarrow 0$, Equations (15a) and (15b):

$$\sigma = \sqrt{1 - \epsilon/2\eta x} \quad (15a)$$

$$e = \pi(n-1/3)x\sigma\eta + 0.5\epsilon \ln[(1 + \sigma)/(1 - \sigma)] \quad (15b)$$

It follows from Equation (15) that the smallest chromophore concentration at which the phase transition occurs equals $x_c = 0.5\epsilon/\eta$ and corresponds to $e = 0$.

An important conclusion follows from Equation (15): The line of the PE to AFE phase transitions depends on the macroscopic shape of the sample. The dashed lines in Figure 7 show the phase transition lines, Equation (15) in the (x, E) plane for the needle ($n=0$), sphere ($n=1/3$), and slab ($n=1$). Figure 7 shows

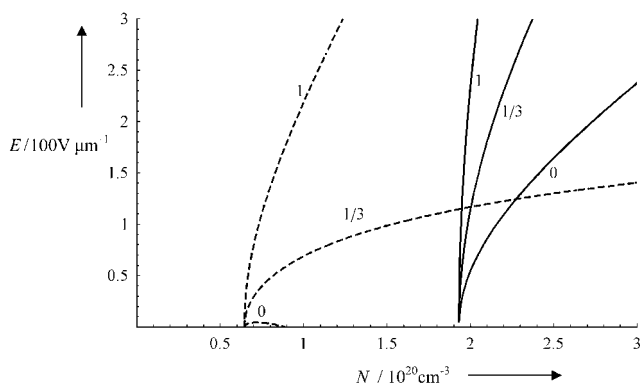


Figure 7. Lines of stability of the PE state in the chromophore concentration–poling field strength coordinate plane (x, E) for the Ising (----) and isotropic (—) models. The data are shown for plate ($n=1$), spherical ($n=1/3$), and needle ($n=0$) shaped samples. Note that the PE state of the Ising model in the needle-shaped sample is unstable only in a small, finite region of the (x, E) plane; $\mu = 10 D$, $T = 373 K$, $\epsilon = 1$.

that the AFE region rapidly decreases with decreasing n . Strictly speaking, the dashed lines describe the region where the PE state becomes unstable and only the AFE state can exist. Complications arise since both first- and second-order phase transitions are possible. A more detailed discussion of the types of phase transitions observed in the Ising model can be found in ref. [36].

The solution of Equations (9) and (14) for the PE and AFE phases for a fixed value of E gives p_z and $r = x\sigma$ as functions of x depicted by the dashed lines in Figures 8 and 9. The data

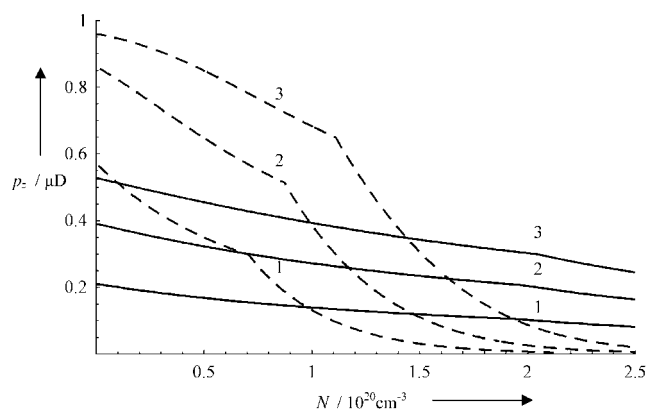


Figure 8. Polarization as a function of chromophore concentration in the plate shaped sample ($n=1$) for three values of E : 1) $100 V \mu m^{-1}$; 2) $200 V \mu m^{-1}$; 3) $300 V \mu m^{-1}$. The cusps in the lines are due to the PE-to-AFE state transition. At low chromophore concentrations, the polarization is greater in the Ising model (----) Equations (9) and (14), whereas at higher chromophore concentrations, past the phase-transition point, the polarization is greater in the isotropic model (—) Equation (21). The parameters are the same as in Figure 7.

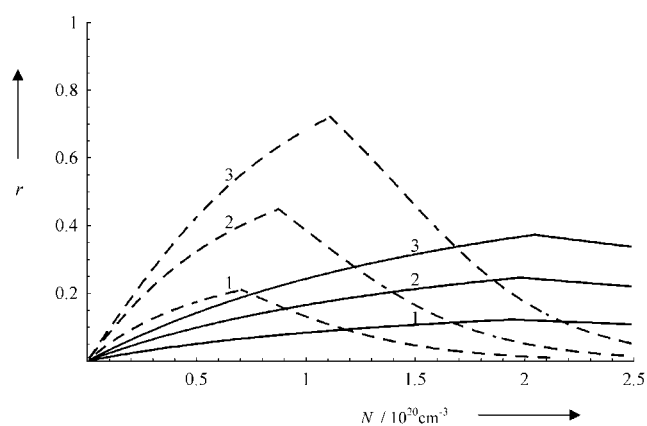


Figure 9. EO coefficient as a function of chromophore concentration in the plate shaped sample ($n=1$) for three values of E : 1) $100 V \mu m^{-1}$; 2) $200 V \mu m^{-1}$; 3) $300 V \mu m^{-1}$. Stronger poling fields produce greater EO coefficients. The maximum values in the EO coefficient are twice as high in the Ising model (----) Equation (10) as they are in the isotropic model (—) Equation (22), and are observed at half the chromophore loadings. The parameters are the same as in Figure 7.

over the whole concentration range show that larger poling fields E result in larger p_z and r . As the concentration increases, the polarization per chromophore p_z decreases, both in the PE and AFE states, while the EO coefficient r increases in the PE state and sharply declines in the AFE state.

Quantitatively, the Ising model is valid only under the assumption that forces stronger than the dipole–dipole interaction force create local liquid-crystalline-like chromophore order, and that the dipole–dipole interaction structure develops in the presence of the spatial order. If the forces creating the spa-

tial order are not strong enough to dominate the dipole-dipole interaction, the two-state Ising space of dipole orientations should be extended.

4. The Isotropic Model

Systems of dipolar chromophores that can take arbitrary orientations in three dimensions, Figure 1c, are described by a complete dipole-dipole Hamiltonian, Equation (16):

$$H = \frac{\mu^2}{8\pi\epsilon_0\epsilon} \sum_{l \neq m} \frac{r_{lm}^2 (\vec{\sigma}_l \cdot \vec{\sigma}_m) - 3(\vec{r}_{lm} \cdot \vec{\sigma}_l)(\vec{r}_{lm} \cdot \vec{\sigma}_m)}{r_{lm}^5} - \frac{\mu E}{\epsilon} \sum_l \sigma_l^z \quad (16)$$

In contrast to the Ising model, the dipole moments of the AFE sublattices in the isotropic model can orient at any angle to the poling field.^[37] A nonzero angle between the dipole moments and the field lowers the thermodynamic potential of the Hamiltonian given by Equation (16). The dipole moments of the AFE sublattices are localized in the (z, x) plane and are symmetric with respect to the z axis, with which they form angles $\pm\vartheta$. Dipole moments along the y axis point in the same direction forming ferroelectric chains. The AFE state of the isotropic model is depicted in Figure 6b and, similarly to the Ising model, is described by two self-consistent effective fields that act on the dipoles of each sublattice.

In the PE state, it is $\theta=0$, and the two effective fields become equivalent. The average z projection of the dipole moment in this state is given by Equation (17):

$$\sigma = (\gamma - \tanh\gamma)/\gamma \tanh\gamma, \quad \gamma = [e - \pi(n-1/3)x\sigma\eta]/\epsilon \quad (17)$$

In the AFE state, the sublattices are polarized at an angle to the external field, Equation (18):

$$\cos\theta = e/\{2\sigma\eta x[1 + (n-1/3)\pi/2]\}^{-1} \quad (18)$$

The average projection of the chromophore dipole on the direction of the sublattice polarization is given by Equation (19):

$$\sigma = (\gamma - \tanh\gamma)/\gamma \tanh\gamma, \quad \gamma = 2\eta\sigma x/\epsilon \quad (19)$$

It follows from Equation (19) that σ in the AFE state of the isotropic model is independent of both the external field and the macroscopic shape of the sample.

Within the space of the external parameters, the regions of PE and AFE states are separated by a second-order phase transition surface in the space of chromophore concentration, poling field strength, macroscopic sample shape, temperature, chromophore dipole, polymer dielectric constant, and other system parameters. The equation for the phase transition surface can be easily found by approaching the phase transition from the AFE side and setting θ to 0, Equation (20):

$$x = \frac{\epsilon\gamma^2 \tanh\gamma}{2\eta(\gamma - \tanh\gamma)}, \quad \gamma = \frac{e}{\epsilon[1 + \pi(n-1/3)/2]} \quad (20)$$

Similar to the Ising model, the phase transition lines obtained with the isotropic model in the concentration-field coordinates depend on the macroscopic sample shape. Independent of the shape, the lines start at the point ($x_c = 1.5\epsilon/\eta$, $e=0$). The critical concentration is three times larger in the isotropic model than in the Ising model. At moderate poling fields, extending to larger fields for slab-shaped samples with $n=1$, the phase transition occurs at higher chromophore concentrations for the isotropic model than for the Ising model: solid and dashed lines in Figure 7, respectively.

Next, consider the expressions for the polarization p_z and EO coefficient $r(x)$ in the isotropic model. The polarization in the PE state equals $p_z = \mu\sigma$ with σ defined in Equation (17). The corresponding expression for the ordered AFE state is Equation (21):

$$p_z = \frac{\mu e}{2\eta x[1 + \pi(n-1/3)/2]} \quad (21)$$

The solid lines in Figure 8 show the functional dependence of p_z on x . At small chromophore concentrations, $x \ll 1$, p_z is much greater in the Ising model than in the isotropic model, but this advantage is rapidly lost with increasing concentration.

The concentration dependence of the EO coefficient $r(x)$ in the PE and AFE states is given respectively by Equations (22a) and (22b):

$$r(x) = x[\sigma(\gamma^2 + 6) - 2\gamma]/\gamma^2 \quad (22a)$$

with σ and γ from Equation (17)

$$r(x) = x \cos\vartheta \{[\sigma(\gamma^2 + 6) - 2\gamma] \cos^2\theta + 3(\gamma - 3\sigma) \sin^2\theta\} / \gamma^2 \quad (22b)$$

with σ , γ , and θ from Equations (18) and (19). The behavior of $r(x)$ with varying concentration x is illustrated in Figure 9 by the solid lines. At the phase transition point, $r(x)$ is maximized. The maximum values of r are smaller in the isotropic model than in the Ising model. The maxima in the isotropic model are shifted to higher chromophore concentrations.

The influence of the macroscopic shape of the sample during poling on $r(x)$ is illustrated in Figure 10 by thick and thin lines for spherical and plate samples, respectively. The data are shown for several values of the poling field. The maximum achievable EO coefficients are over two-fold larger for spherical samples than for plate samples. Figure 10 illustrates that a favorable choice of sample shape for poling can lead to a substantially better EO response of the final material. The most common poling of films is least favorable. The best EO response will be achieved when poling is carried out with samples elongated in the direction the poling field.

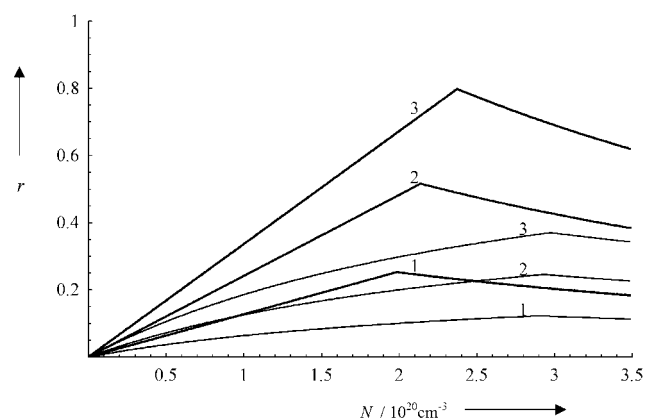


Figure 10. EO coefficient as a function of chromophore concentration in the isotropic model for three values of E : 1) $100 \text{ V } \mu\text{m}^{-1}$; 2) $200 \text{ V } \mu\text{m}^{-1}$; 3) $300 \text{ V } \mu\text{m}^{-1}$. The bold solid lines correspond to spherical samples; the thin solid lines represent plate samples. Poling of spherical samples is more efficient. $\mu = 10 \text{ D}$, $T = 373 \text{ K}$, $\epsilon = 1$. For clarity, and to avoid data overlap, the maxima for the plate were shifted by choosing $\epsilon = 1.5$.

5. Discussion and Comparison with Experiment

The theoretical models for the dependence of the EO coefficient on chromophore loading are compared with the experimental data for the four well-studied guest–host systems, the CLD-H, FTC-H, GLD-H, and ISX chromophores, Figure 11. The dipole moments of these quasilinear molecules equal 13.47, 12.19, 13.88, and 8 D,^[10–14] respectively. The focus is on the concentration dependence of the EO coefficient r , and the data are given in a normalized form, similar to the experimental data.^[10–14] The chromophores were dissolved in a melted polymer at 100°C , spin-coated into a film and poled by an electric field of $E = 100 \text{ V } \mu\text{m}^{-1}$ between plate electrodes, corresponding to a sample shape depolarization parameter $n = 1$. The dielectric constant of the polymer matrix ϵ was of the order of two. This value was slightly adjusted to better match the theoretical and experimental maxima in the EO coefficient. Larger values of ϵ shift the EO maximum to higher chromophore concentrations.

Figure 11 a compares the normalized r of the CLD-H chromophore system obtained theoretically and experimentally. Good

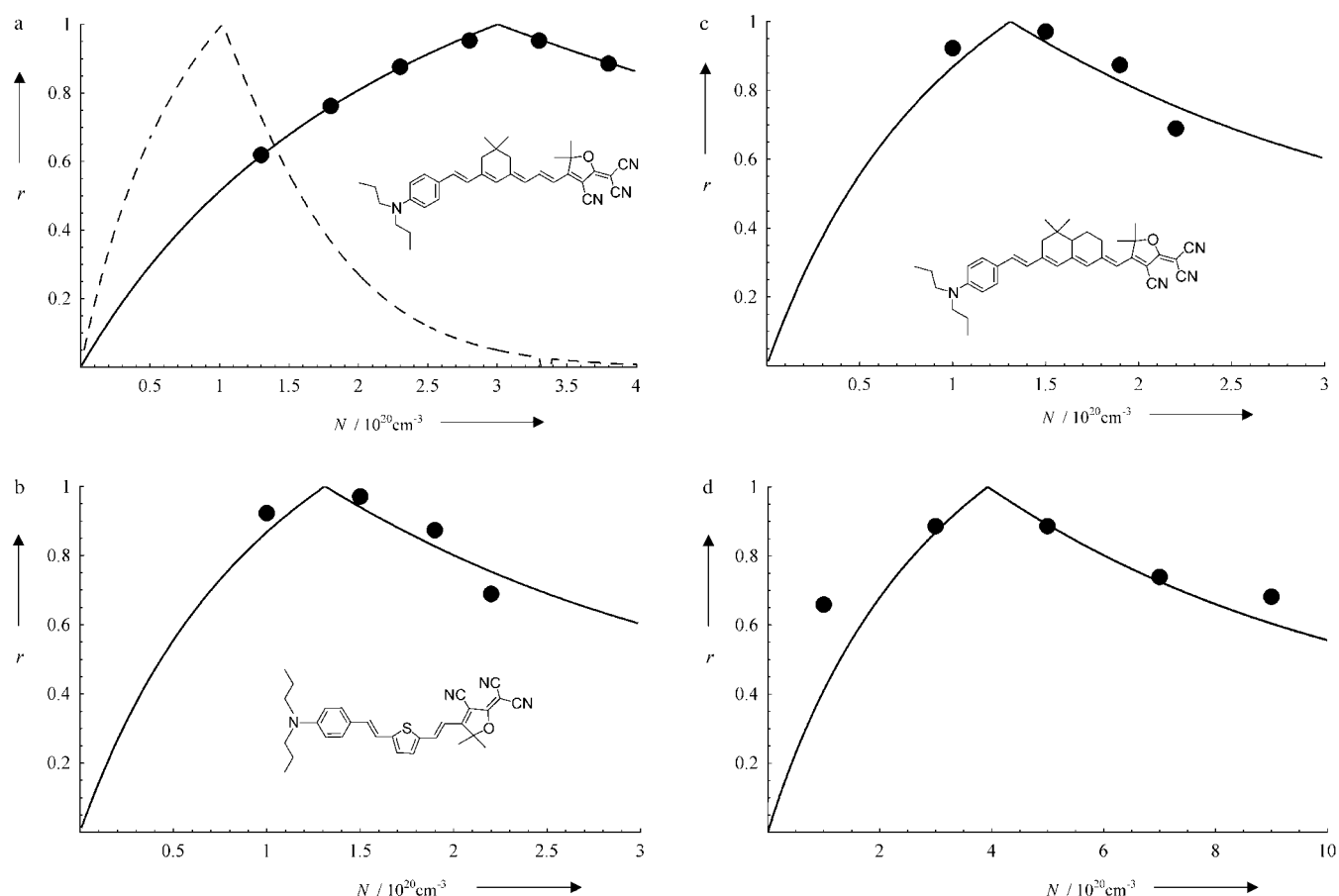


Figure 11. Comparison of the computed normalized EO coefficient with the experimental data for a) CLD, b) FTC, c) GLD, and d) ISX chromophores. Circles represent the experimental data, solid lines correspond to the isotropic model, and the dashed line is computed with the Ising model. The isotropic model shows excellent agreement with the experimental data, whereas the Ising model underestimates the AFE phase-transition concentrations. The data are shown for a poling field of $100 \text{ V } \mu\text{m}^{-1}$, poling temperature $T = 373 \text{ K}$, and plate-shaped sample with $n = 1$. The dipole moments were taken from refs. [10–14]. a) $\mu = 13.47 \text{ D}$, $\epsilon = 2.82$; b) $\mu = 12.149 \text{ D}$, $\epsilon = 1.0$; c) $\mu = 13.88 \text{ D}$, $\epsilon = 1.7$; d) $\mu = 8.0 \text{ D}$, $\epsilon = 1.3$.

agreement is observed with the isotropic model. The Ising model reproduces the overall shape of the experimental data and can be shifted to match the experimental maximum by a significant increase of ϵ .^[34] Similar discrepancies between the peaks of the experimental data and the Ising curves were observed with the other systems, while the isotropic model remains in good agreement with experiment. An agreement between the Ising model and experiment can also be achieved if the dipole axis is tilted at an angle to the longest molecular axis.^[19] Computational studies of a variety of chromophores confirmed this possibility.^[51] Although agreement between the experimental data and the Ising model can be achieved by adjusting a single parameter—either the polymer dielectric constant^[34] or the angle of the chromophore dipole^[19]—for clarity only the isotropic model results are presented for the FTC-H, GLD-H, and ISX chromophore systems, Figures 11 b, 11 c, and 11 d. Good agreement between theory and experiment was seen in all cases.

The comparison between the experimental and theoretical data indicates that models of dipolar systems invoking a phase transition between the PE and AFE states produce a successful quantitative description of the EO coefficient and its dependence on chromophore loading. The maximum of the EO coefficient is achieved at the phase transition point. At low chromophore concentrations, the system of dipoles exists in the PE state, and the EO coefficient grows with concentration. Increasing the chromophore loading favors AFE correlations between dipoles and ultimately results in the AFE phase transition. Once the system switches into the AFE state, the dipolar polarization and the EO coefficient rapidly decay even in strong poling fields.

6. Conclusions

A systematic analysis of the factors that determine the magnitude of the EO coefficient in polymeric NLO materials has been presented. The EO coefficient not only defines the quality of the material for specific EO devices, but characterizes the potential of the material for other NLO applications as well.

The theoretical analysis shows that large values of the EO coefficient can be obtained in systems, where the space of orientations available to chromophore dipoles is significantly restricted. Any constraint that aligns chromophore dipoles in the preferred direction favors efficient poling and, therefore, leads to larger EO coefficients. For instance, the maximum values of the EO coefficient achievable for Ising dipoles are about twice as high as those achievable for isotropic dipoles.

The shape of the chromophore molecule is another important characteristic that can be tuned to produce local chromophore arrangements favoring ferroelectric correlations between chromophore dipoles. In particular, poling best aligns oblate ellipsoid chromophores with dipole moments pointing along the shortest ellipsoid axis.

The macroscopic shape of the chromophore–polymer sample subjected to the external poling field substantially alters the magnitudes of the electric polarization and EO coefficient due to the long range of the dipole–dipole interaction.

Rod-shaped samples with the poling field directed along the rod axis produce the best EO coefficients. Most experimental poling procedures are applied to polymer films, which are least favorable for poling. Poling of samples elongated in the poling field direction, for example in cylindrical pores, would be more efficient.

Larger values of chromophore dipoles allow for better poling. Chemical bonding of several chromophores into a block with a large total dipole increases the EO coefficient. This effect is observed in dendrimers,^[27] as elucidated in ref. [19].

Two models have been considered in detail. The Ising model allows for only two orientations of chromophore dipoles, whereas the isotropic model considers all possible angular orientations. Both models predict phase transitions into AFE states with increasing chromophore concentration. The AFE phase transition results in a sharp decline of the EO response. The phase transition occurs at higher chromophore concentrations in the isotropic model than in the Ising model. The maximum values in the EO coefficient are twice as high in the Ising model as they are in the isotropic model, and occur at half the chromophore loading. The experimental data for the systems considered in this study are best described with the isotropic dipole model.

Acknowledgements

The research was supported by the NSF, CAREER Award CHE-0094012 and Materials and Devices for Information Technology STC. OVP is an Alfred P. Sloan Fellow and is grateful to Professor Daniel Borgis at the Laboratoire de Physique Théorique des Liquides, Université Pierre et Marie Curie, Paris, France for hospitality during manuscript preparation.

Keywords: chromophores • nonlinear optics • phase transitions • poling processes • polymers

- [1] *Nonlinear Optical Properties of Organic and Polymeric Materials* (Ed.: D. J. Williams), ACS Symp. Ser. 233, American Chemical Society, Washington, D.C., 1983.
- [2] R. S. Gopalan, G. U. Kulkarni, C. N. R. Rao, *ChemPhysChem* **2000**, *1*, 127–135.
- [3] F. Wurthner, R. Wortmann, K. Meerholz, *ChemPhysChem* **2002**, *3*, 17–31.
- [4] O. Ostroverkhova, M. He, R. J. Twieg, W. E. Moerner, *ChemPhysChem* **2003**, *4*, 732–744.
- [5] S. R. Marder, L. T. Cheng, B. G. Tiemann, A. C. Friedli, M. Blanchard-Desce, J. W. Perry, J. Skindhoj, *Science* **1994**, *263*, 511–514.
- [6] F. Hide, B. J. Schwartz, M. A. Diaz-Garcia, A. J. Heeger, *Synth. Met.* **1997**, *91*, 35–40.
- [7] I. G. Voigt-Martin, G. Li, U. Kolb, H. Kothe, A. V. Yakimanski, A. V. Tenkovtsev, C. Gilmore, *Phys. Rev. B* **1999**, *59*, 6722–6735.
- [8] J. Cornil, D. Beljonne, J. P. Calbert, J. L. Bredas, *Adv. Mater.* **2001**, *13*, 1053–1067.
- [9] E. E. Neuteboom, S. C. J. Meskers, P. A. van Hal, J. K. J. van Duren, E. W. Meijer, R. A. J. Janssen, H. Dupin, G. Pourtois, J. Cornil, R. Lazzaroni, J. L. Bredas, D. Beljonne, *J. Am. Chem. Soc.* **2003**, *125*, 8625–8638.
- [10] A. W. Harper, S. Sun, L. R. Dalton, S. M. Garner, A. Chen, S. Kalluri, W. H. Steier, B. H. Robinson, *J. Opt. Soc. Am. B* **1998**, *15*, 329–337.
- [11] B. H. Robinson, L. P. Dalton, A. W. Harper, A. Ren, F. Wang, C. Zhang, G. Todorova, M. Lee, R. Aniszfeld, S. Garner, A. Chen, W. H. Steier, S. Hou-

- brecht, A. Persoons, I. Ledoux, J. Zyss, A. K. Y. Jen, *Chem. Phys.* **1999**, *245*, 35–50.
- [12] A. K. Y. Jen, Y. Q. Liu, L. X. Zheng, S. Liu, K. Y. Drost, Y. Zhang, L. R. Dalton, *Adv. Mater.* **1999**, *11*, 452–455.
- [13] Y. Shi, C. Zhang, H. Zhang, J. H. Bechtel, L. R. Dalton, B. H. Robinson, W. H. Steier, *Science* **2000**, *288*, 119–122.
- [14] B. H. Robinson, L. R. Dalton, *J. Phys. Chem. A* **2000**, *104*, 4785–4795.
- [15] F. Kajzar, K.-S. Lee, A. K.-Y. Jen, *Adv. Polym. Sci.* **2003**, *161*, 1–85.
- [16] S. Yokoyama, T. Nakahama, A. Otomo, S. Mashiko, *J. Am. Chem. Soc.* **2000**, *122*, 3174–3181.
- [17] C. H. Wang, J. N. Woodford, C. Zhang, L. R. Dalton, *J. Appl. Phys.* **2001**, *89*, 4209–4217.
- [18] K. Clays, E. Hendricks, T. Verbiest, A. Persoons, *Adv. Mater.* **1998**, *10*, 643–655.
- [19] Y. V. Pereverzev, O. V. Prezhdo, L. R. Dalton, *Chem. Phys. Lett.* **2003**, *373*, 207–212.
- [20] B. K. Mandal, Y. M. Chen, J. Y. Lee, J. Kumar, S. Tripathy, *Appl. Phys. Lett.* **1991**, *58*, 2459–2460.
- [21] D. M. Zhang, J. Z. Sun, J. C. Shen, M. B. Yi, *J. Appl. Polym. Sci.* **2000**, *77*, 1506–1512.
- [22] T. L. Penner, J. S. Schildkraut, H. Ringsdorf, A. Schuster, *Macromolecules* **1991**, *24*, 1041–1049.
- [23] J. P. Cresswell, M. C. Petty, J. E. Shearman, S. Allen, T. G. Ryan, I. Ferguson, *Thin Solid Films* **1994**, *224*, 1067–1072.
- [24] D. Beyer, W. Paulus, M. Seitz, G. Maxein, H. Ringsdorf, M. Eich, *Thin Solid Films* **1995**, *271*, 73–83.
- [25] E. Milko, M. E. van der Boom, G. Evmenenko, P. Dutta, T. J. Marks, *Adv. Funct. Mater.* **2001**, *11*, 393–397.
- [26] A. Facchetti, A. Abbotto, L. Beverina, M. E. van der Boom, P. Dutta, G. Evmenenko, G. A. Pagani, T. J. Marks, *Chem. Mater.* **2003**, *15*, 1064–1072.
- [27] H. Ma, S. Liu, J. D. Luo, S. Suresh, L. Liu, S. H. Kang, M. Haller, T. Sassa, L. R. Dalton, A. K. J. Jen, *Adv. Funct. Mater.* **2002**, *12*, 565–574.
- [28] B. K. So, K. S. Lee, S. M. Lee, M. K. Lee, T. K. Lim, *Opt. Mater.* **2003**, *21*, 87–92.
- [29] W. J. Kuo, G. H. Hsiue, R. J. Jeng, *Macromol. Rapid Commun.* **2001**, *22*, 601–606.
- [30] T. Kimura, T. Fukuda, H. Matsuda, A. Komoriya, M. Kazama, M. Kato, S. Okada, H. Nakanishi, *Polym. Adv. Technol.* **2001**, *12*, 231–236.
- [31] C. Zhang, C. G. Wang, L. R. Dalton, H. Zhang, W. H. Steier, *Macromolecules* **2001**, *34*, 253–261.
- [32] D. Bosc, F. Foll, B. Boutevin, A. J. Rousseau, *J. Appl. Polym. Sci.* **1999**, *74*, 974–982.
- [33] O. K. Kim, L. S. Choi, H. Y. Zhang, X. H. He, Y. T. Shih, *Thin Solid Films* **1998**, *327*, 172–175.
- [34] Y. V. Pereverzev, O. V. Prezhdo, *Phys. Rev. E* **2000**, *62*, 8324–8334.
- [35] Y. V. Pereverzev, O. V. Prezhdo, L. R. Dalton, *Chem. Phys. Lett.* **2001**, *340*, 328–335.
- [36] Y. V. Pereverzev, O. V. Prezhdo, L. R. Dalton, *Phys. Rev. B* **2002**, *65*, Art. No. 052104.
- [37] Y. V. Pereverzev; O. V. Prezhdo; L. R. Dalton, *J. Chem. Phys.* **2002**, *117*, 3354–3360.
- [38] A. Berardi, L. Muccioli, C. Zannoni, *ChemPhysChem* **2004**, *5*, 104–111.
- [39] F. Wurthel, S. Yao, T. Debaerdemaeker, R. Wortmann, *J. Am. Chem. Soc.* **2002**, *124*, 9431–9447.
- [40] S. H. L. Klapp, G. N. Patey, *J. Chem. Phys.* **2001**, *115*, 4718–4731.
- [41] S. T. Lagerwall, *J. Phys.: Condens. Matter* **1996**, *8*, 9143–9166.
- [42] P. I. C. Teixeira, J. M. Tavares, M. M. Telo da Gama, *J. Phys.: Condens. Matter* **2000**, *12*, R411–R434.
- [43] J. M. Luttinger, L. Tisza, *Phys. Rev.* **1946**, *70*, 954–964.
- [44] C. Kittel, *Introduction to Solid State Physics*, Wiley, New York, **1996**.
- [45] D. Levesque, J. J. Weis, G. J. Zarragoicochea, *Phys. Rev. E* **1993**, *47*, 496–505.
- [46] A. I. Akhiezer, V. G. Baryakhtar, S. V. Peletminskii, *Spin Waves*, North-Holland, Amsterdam, **1968**.
- [47] B. E. Vugmeister, H. Rabitz, *J. Stat. Phys.* **1997**, *88*, 471–486.
- [48] A. G. Anders, S. V. Volotskii, S. V. Startsev, A. Feger, A. Orendacheva, *Low Temp. Phys.* **1995**, *21*, 52–60.
- [49] J. S. Smart, *Effective Field Theories of Magnetism*, Saunders, Philadelphia, **1966**.
- [50] A. A. Loginov, Y. V. Pereverzev, *Low Temp. Phys.* **1998**, *24*, 652–660.
- [51] O. V. Prezhdo, *Adv. Mater.* **2002**, *14*, 597–600.

Received: February 12, 2004

Early View Article

Published online on November 17, 2004